

The effects of Ge content on the microstructure and specific contact resistance of solid-state NiAuGe/ZrB₂/Au ohmic contacts to n-InGaAs

J. S. YU, A. E. STATON-BEVAN

Department of Materials, Imperial College of Science, Technology and Medicine, University of London, London SW7 2BP, UK

J. HERNIMAN*, D. A. ALLAN

British Telecom Laboratories, Martlesham Heath, Ipswich, IP5 7RE, UK

The Ge thickness, x , of NiAuGe(5 nm / 45 nm / x nm)/ZrB₂(50 nm)/Au(20 nm) ohmic contacts to n-InGaAs was varied between 0 and 20 nm. The microstructures of these contacts, after annealing at 270 °C, were investigated using transmission electron microscopy (TEM) and correlated with the respective specific contact resistances. In the absence of Ge, a Ni–Ga–As phase was formed at the metal–semiconductor interface and the specific contact resistance was high (0.63 Ω mm). When thicknesses of $x = 10$ nm or $x = 15$ nm of Ge were added, Ni–Ge–As phases were observed, but they were replaced by AuGeAs and NiGe when $x = 20$ nm. The specific contact resistance was a minimum (0.11 Ω mm) for this composition. Ge was clearly beneficial for ohmic-contact formation. The low-temperature I – V characteristics of the contact containing the largest amount of Ge (that is, $x = 20$ nm) indicated that electron tunnelling through degenerately-Ge-doped regions was not the dominant ohmic mechanism in these contacts.

1. Introduction

In optoelectronic integrated circuits (OEICs), optical components (for example, laser diodes or photodetectors) and electronic transistors (for example, field-effect transistors, bipolar-junction transistors) are monolithically integrated onto a single substrate. This has many advantages over the conventional hybrid circuits, including multifunction capabilities, and a reduction in the overall number of devices. Most importantly, OEICs provide enhanced speed and improved noise performance due to the elimination of parasitic elements arising from bonding wires and pads [1, 2]. To exploit these advantages to the full, a suitably low-resistance ohmic contact is required.

There are two types of OEIC – short wavelength circuits (that is, 0.88–0.91 μm) based on GaAs and its related compounds, and long wavelength circuits (that is, 0.92–1.65 μm) based on InP and its related compounds. The latter are better suited for long distance, single-mode telecommunications because they are able to produce, and operate at, the minimum-signal-attenuation wavelengths of 1.32 μm and 1.55 μm [3]. In_{0.53}Ga_{0.47}As, lattice matched to InP, is essential for the fabrication of the electron transistors and photodiodes of long-wavelength OEICs. In this study, the NiAuGe/ZrB₂/Au system, originally developed for ohmic contacts to n-GaAs [4], is investigated as a

possible ohmic contact to n-InGaAs. For n-GaAs, the contacts are normally *alloyed* at ~ 440 °C, above the melting point of the metallization, and the contact microstructure forms during resolidification. For the contacts to n-InGaAs investigated in the present study, however, ohmic contacts were produced by annealing at 270 °C, therefore, the contact reaction took place via *solid-state* diffusion.

The minimum layer thickness in the OEIC devices being developed is 100 nm. Penetration by the metallization into the semiconductor during annealing should be less than this value. Specific-contact-resistance values less than 0.5 Ω mm are acceptable, but a lower resistance value is desirable.

The effects of the annealing temperature and the Ni content for these contacts have been published by the authors elsewhere [5]. It was demonstrated that (i) interfacial NiGe increases the contact resistance, while AuGeAs is beneficial; and (ii) the Ni acts as a catalyst to AuGeAs formation. The present paper aims to complete the characterization of this contact by studying the effects of Ge content.

2. Experimental procedure

2.1. Contact fabrication

The contact-layer structure is shown in Fig. 1. The contact metals, a ZrB₂ diffusion barrier and an Au

*Present address: BT & D Technologies, Whitehouse Road, Ipswich, Suffolk, IP1 5PB, UK.

TABLE I NiAuGe (5 nm/45 nm/x nm)/ZrB₂(50 nm)/Au(20 nm) ohmic contacts to the n-InGaAs investigated in this study and their specific resistance values, $r_c(\Omega \text{ nm})$.

| Specimen | Ge content x (nm) | Annealing temp (°C) | Specific contact resistance $r_c(\Omega \text{ nm})$ | STD ($\Omega \text{ nm}$) |
|----------|------------------------|------------------------|---|--------------------------------|
| S1 | 0 | 270 | 0.63 | 0.23 |
| S2 | 10 | 270 | 0.17 | 0.06 |
| S3 | 15 | 270 | 0.28 | 0.08 |
| A1 | 20 | As-deposited | 0.30 | 0.05 |
| S4 | 20 | 270 | 0.11 | 0.06 |

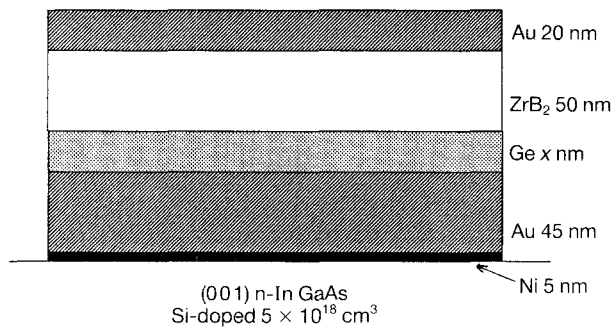


Figure 1 Schematic diagram of the as-deposited contacts to n-InGaAs, NiAuGe (5 nm/45 nm/x nm)/ZrB₂(50 nm)/Au(20 nm), where $0 \leq x \leq 20$ nm.

overlayer were sequentially deposited on molecular beam epitaxy- (MBE)-grown (001) n-In_{0.53}Ga_{0.47}As (Si-doped, $N_d \sim 5 \times 10^{18} \text{ cm}^{-3}$) on InP, using electron-beam evaporation at $< 10^{-6}$ Pa. The Ni and Au layers were kept at 5 nm and 45 nm, respectively, while the Ge layer thickness was varied from 0 to 20 nm (Table I). The annealing was performed using a graphite strip heater. The ramping-up time from room temperature to 270 °C was approximately 30 s. The temperature was held for 2 s and then the contacts were allowed to cool.

2.2. Electrical measurements

2.2.1. Transmission-line model measurements

The specific contact resistance, r_c , was measured using the transmission line model (TLM) method. The TLM patterns were prepared by conventional photolithographic techniques and consisted of five $100 \times 150 \mu\text{m}^2$ pads separated by spaces of 5, 10, 15 and 20 μm . The specific contact resistance measurements were performed using a programmable direct-current (d.c.) parametric tester, with an automatic stepping prober.

2.2.2. I - V characteristics

The current-voltage, (I - V), characteristics of the as-deposited and annealed contacts containing 20 nm thick Ge layers (specimens A1 and S4) were measured at room temperature, at 150 K and at 100 K.

2.3. Transmission electron microscopy

Plan-view transmission electron microscopy (TEM) specimens were prepared by grinding from the substrate side, dimple polishing with 1 μm diamond paste and chemical thinning with a bromine-methanol mixture (0.5 vol % of Br), followed by a brief Ar⁺ ion beam milling at 4.5 kV with an incident angle of 15°.

Cross-sectional TEM specimens were prepared by standard techniques, using Ar⁺ milling at 4.5 kV with an incident angle of 13°. All the specimens were Ar⁺ milled using a liquid-nitrogen-cooled specimen stage. Jeol Temscan 120CX and 2000FX microscopes were used for most of the TEM work. A Jeol JEM 2010 was used for 3 nm probe-size EDAX (EnergyDispersive Analysis by X-rays). The TEM EDAX results could only be treated semi-quantitatively since the X-ray signals collected from the thin-foil specimens were insufficient for the analysis to be statistically meaningful.

3. Results and discussion

3.1. Contact microstructures

3.1.1. Microstructure of the as-deposited contact A1: NiAuGe (5 nm/45 nm/20 nm)/ZrB₂(50 nm)/Au(20 nm)

The microstructure of an as-deposited contact, containing a 20 nm thick layer of Ge, was initially examined. The top Ge layer remained amorphous and undiffused. The intermediate Au layer was polycrystalline with an average grain diameter of approximately 40 nm. The Ni layer showed good adhesion to the InGaAs in contact with it, but it had not reacted to any detectable extent: that is, there had been negligible reaction during metal deposition.

3.1.2. Microstructure of contacts annealed at 270 °C

A schematic summary of the microstructures of the four annealed contacts, containing 0, 10, 15 and 20 nm Ge layers, is given in Table II.

3.1.2.1. Microstructure of the contact containing no Ge, contact S1: NiAu(5 nm/45 nm)/ZrB₂(50 nm)/Au(20 nm). A plan-view TEM micrograph of the metallization of this contact is shown in Fig. 2a. The Au grains had grown on annealing, the majority being between 50 and 200 nm in diameter. These grains, which contained small amounts of In (~7 at%) and Ga (~5 at%), contained a large number of planar defects which gave rise to streaking in the diffraction pattern (Fig. 2b). These planar defects are thought to be plate-like precipitates of Au₉In₄ or α' Au-Ga. (001) plates of α' Au-Ga, have been observed lying parallel to {111} planes in cubic α Au(Ga), in Au-Ge contacts to n-GaAs [6]. Certain grains which were considerably larger than the surrounding grains had a particularly high density of these defects. An example of such a grain, which is 400 nm in diameter, may be seen in Fig. 2a.

TABLE II Summary of the effects of the Ge content, x , on the microstructure and specific contact resistance of NiAuGe (5 nm/45 nm/ x nm)/ZrB₂ (50 nm)/Au (20 nm) ohmic contacts to n-InGaAs annealed at 270 °C

| | No Ge:S1 | 10 nm Ge:S2 | 15 nm Ge:S3 | 20 nm Ge:S4 |
|-----------------------------|---|--|---|---|
| | | | | |
| Specific contact Resistance | 0.63 Ω mm | 0.17 Ω mm | 0.28 Ω mm | 0.11 Ω mm |
| Au grain | 150 nm average up to 200 nm | up to 200 nm | up to 200 nm | up to 200 nm |
| | ← | less than 12 at% of In + Ga | → | < 12 at% In |
| | Abnormal growth of some grains containing a high density of plate-shaped defects; ~ 400 nm 2nd phase ppt. | | | |
| Au penetration Ge | 20 nm Not present | 160 nm No elemental Ge | 80 nm < 40 nm at Au grain boundaries | 50 nm 60 nm at Au grain boundaries |
| Ni phases | Ni-Ga-As at the metal-semiconductor interface: ~ 2:1:2? | Ni ₂ GeAs ~ 100 nm No NiGe | Ni-Ge-As: from 1:1:1 to 3:3:4 or 3:4:3 NiGe at the metal-semiconductor interface | NiGe at the metal-semiconductor interface |
| AuGeAs | None | Very few | Occasional; 200 nm | Readily observed 300 nm ^a |

^a Not shown in diagram; observed in plan view

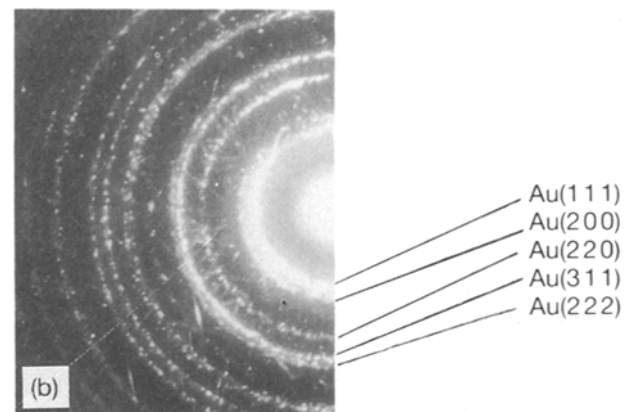
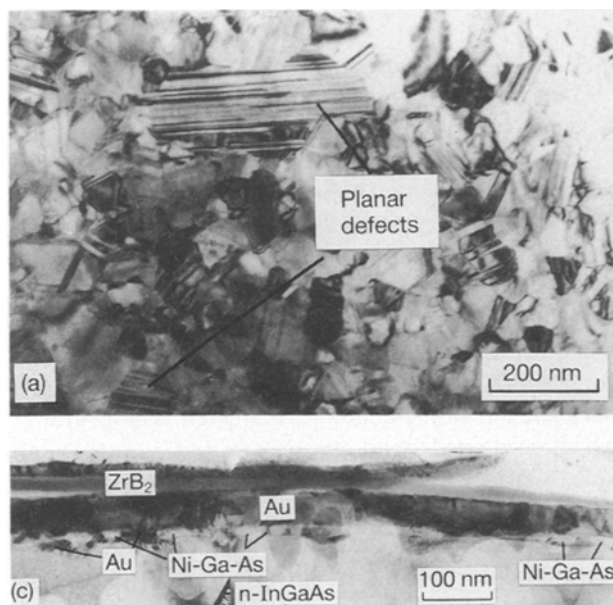


Figure 2 Microstructure of the 270 °C annealed contact with no Ge, contact S1: NiAu (5 nm/45 nm)/ZrB₂ (50 nm)/Au (20 nm): (a) TEM BF plan view (b) SADP from plan view and (c) TEM BF cross-sectional view.

Cross-sectional TEM showed an interfacial Ni-Ga-As phase (Fig. 2c). Its coverage was extensive but not continuous, occasionally being broken by Au grains. Both phases penetrated the semiconductor to a depth of ~ 20 nm.

When EDAX was performed on the Ni-Ga-As phase, the ratio of Ni:Ga:As was approximately 2:1:2. This matches none of the Ni-Ga-As compositions reported previously, that is, Ni₂GaAs [7, 8] or Ni₃GaAs [9]. Ni-Ga-As phases, however, have been reported to increase the contact resistance [7]. The Ni-Ga-As phase observed in the present work may,

therefore, have contributed to the high specific contact resistance of this contact ($r_c = 0.63 \Omega \text{ mm}$).

3.1.2.2. Microstructure of the contact containing $x = 10 \text{ nm}$ of Ge, contact S2: NiAuGe(5 nm/45 nm/10 nm)/ZrB₂(50 nm)/Au(20 nm). TEM micrographs of specimen S2 are shown in Fig. 3. The introduction of a 10 nm Ge layer resulted in the formation of Ni₂GeAs islands between the Au grains, Fig. 3a. Previously this phase had only been observed in alloyed contacts annealed above 400°C [6, 10, 11]. Ni₂GeAs has a hexagonal structure with identical lattice spacings to NiAs ($a = 0.3609 \text{ nm}$, $c = 0.5109 \text{ nm}$) [6]. Very occasionally, monoclinic AuGeAs and a second Ni–Ge–As phase were also observed. (Incidentally, this second Ni–Ge–As phase was readily observed in the contact containing 15 nm of Ge.) There was no trace of any Ge rings in the diffraction pattern, implying that all the Ge was consumed in the formation of Ni–Ge–As phases. The metal–semiconductor interface was rough Fig. 3b). The Au penetration into the semiconductor was as deep as 160 nm, which is larger than the minimum layer thickness of 100 nm required for OEIC devices.

3.1.2.3. Microstructure of the contact containing $x = 15 \text{ nm}$ of Ge, contact S3: NiAuGe(5 nm/45 nm/15 nm)/ZrB₂(50 nm)/Au(20 nm). Increasing the Ge layer thickness by 5 nm resulted in an entirely different microstructure from specimen S2. The Ni–Ge–As phase of composition Ni₂GeAs was replaced by needles of composition Ni:Ge:As $\sim 1:1:1$ (Fig. 4a). These Ni–Ge–As grains were typically 300–400 nm long. They lay at an angle to the semiconductor surface, making any epitaxial relationship with the InGaAs unlikely. According to EDAX studies, the Ni–Ge–As contained less Ni (or more Ge and As) than Ni₂GeAs. The Ni:Ge:As ratio varied from approximately 1:1:1 to As-rich 3:3:4 or Ge rich 3:4:3. In addition to the Ni–Ge–As phase, some un-

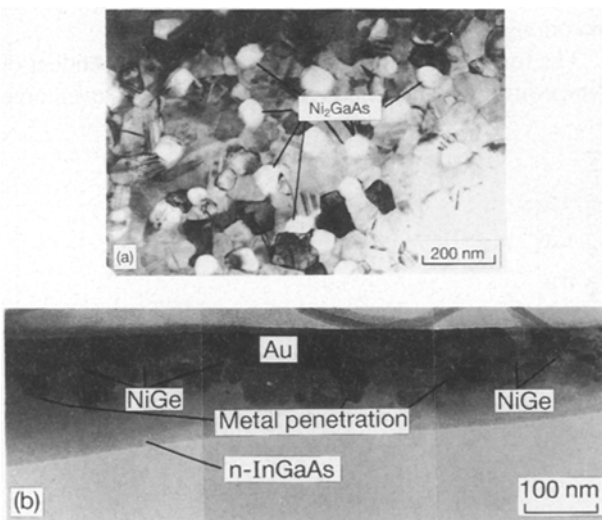


Figure 3 Microstructure of the 270°C annealed contact with 10 nm of Ge, contact S2: NiAuGe (5 nm/45 nm/10 nm)/ZrB₂(30 nm)/Au(20 nm) (a) TEM BF plan view of typical metallization, and (b) TEM BF cross-sectional view (part of the diffusion barrier and the top Au layer have been removed).

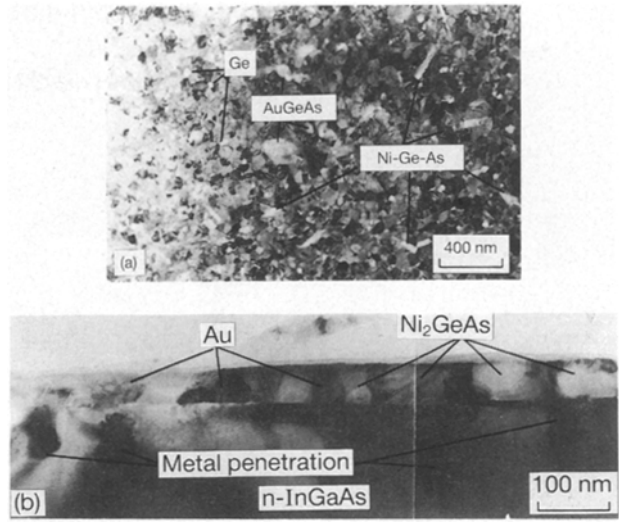


Figure 4 Microstructure of the 270°C annealed contact with 15 nm of Ge, contact S3: NiAuGe (5 nm/45 nm/15 nm)/ZrB₂(50 nm)/Au(20 nm) (a) TEM low magnification plan view, and (b) TEM BF cross-sectional view showing an interface region where the NiGe formation was incomplete and metal penetration into the semiconductor was extensive.

reacted Ge formed islands, $\sim 40 \text{ nm}$ in diameter, at the Au grain boundaries. Small AuGeAs crystals were also occasionally observed.

Orthorhombic NiGe was present at the metal–semiconductor interface. Cross-sectional examination revealed that where the NiGe phase was continuous, the metal–semiconductor interface was smooth, with little metal penetration into the InGaAs. However, where the NiGe coverage was incomplete, the metalization penetrated $\sim 80 \text{ nm}$ into the semiconductor. Such a region is shown in the cross-section of Fig. 4b. This observation, that NiGe acts as a barrier to metal penetration, supports the results of previous work published elsewhere [5]. NiGe is, therefore, beneficial from a microstructural point of view, however, its electrical properties are thought to be detrimental to good ohmic-contact formation [5].

3.1.2.4. Microstructure of the contact containing $x = 20 \text{ nm}$ of Ge, contact S4: NiAuGe(5 nm/45 nm/20 nm)/ZrB₂(50 nm)/Au(20 nm). TEM micrographs of this contact are shown in Fig. 5. With the higher Ge content, the Ni–Ge–As phase was no longer present. Instead, the amount of AuGeAs had increased, both in the number of grains and their size (Fig. 5a). The average grain size was approximately 300 nm in diameter. When the Au metallization was etched away using a KI solution, the AuGeAs phase was found on the surface of the InGaAs epilayer, suggesting that this phase had nucleated at the metal–semiconductor interface and grown into the metallization. Auvray *et al.* in [12] and Kim and Chung [13] have reported (different) epitaxial relationships between AuGeAs and InGaAs. Elemental traces of Ni were found in the vicinity of the AuGeAs crystals. This suggests that Ni plays an important role in the formation of AuGeAs, supporting previous results from the microstructural study of the contacts with various Ni contents [5].

Increasing the Ge layer thickness from 15 nm to 20 nm resulted in an increase in the Ge island dia-

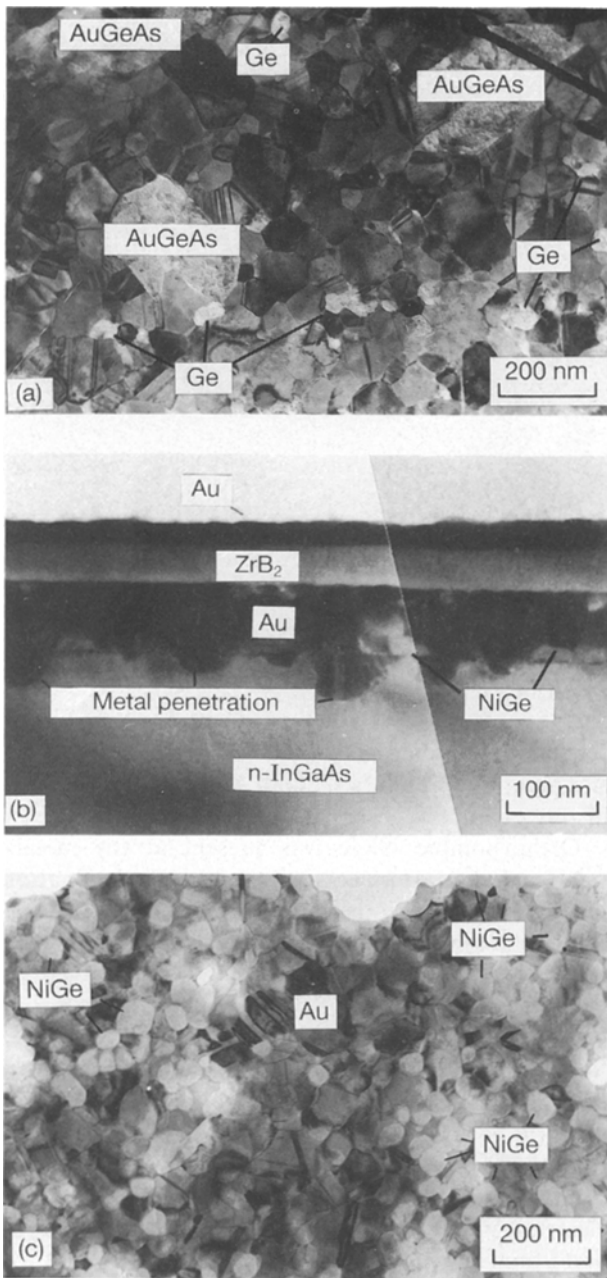


Figure 5 Microstructure of the 270°C annealed contact with 20 nm of Ge, contact S4: NiAuGe (5 nm/45 nm/20 nm)/ZBr₂(50 nm)/Au(20 nm) (a) TEM BF plan view of the metallization, (b) TEM BF cross-sectional view, and (c) TEM BF plan view of the interfacial region after Ar⁺ Milling from the contact side reveal the NiGe grains.

meter from ~ 40 nm to ~ 60 nm. For the high Ge-content contact, the TEM cross-section (Fig. 5b) showed that the metal–semiconductor interface was smooth apart from occasional Au penetrations into the semiconductor which could be as deep as ~ 50 nm. NiGe tended to form small clusters of several grains rather than individual grains at the metal–semiconductor interface (Fig. 5c).

Au grains invariably contained more In than Ga. This was in contrast to the contacts containing 0–15 nm thick layers of Ge, in which, Au grains sometimes contained a greater or comparable amount of Ga (Table II). A difference between the two groups of contacts was that, in the former, Ni only acted as a catalyst, assisting the dissociation of weaker In–As

bonds in preference to stronger Ga–As bonds. In the latter, Ni actively reacted with the InGaAs forming Ni–Ga–As phases, with little discrimination between attacking In–As or Ga–As bonds.

3.2. Electrical measurements

3.2.1. Specific contact resistance, r_c

The specific contact resistance, r_c , of the as-deposited and alloyed contacts, as a function of Ge content, is shown in Fig. 6.

The as-deposited contact A1 (which TEM showed to have an unreacted, layered microstructure (Section 3.1.1.)) was ohmic ($r_c = 0.30 \pm 0.05 \Omega \text{ mm}$).

For the alloyed contacts S1–S4, the contact with no Ge had the highest resistance, $r_c = 0.63 \pm 0.23 \Omega \text{ mm}$. The addition of Ge decreased this value considerably. Ge is therefore beneficial for ohmic properties. The minimum specific contact resistance of $0.11 \pm 0.06 \Omega \text{ mm}$ was obtained for the contact with 20 nm of Ge, that is, contact S4.

Determining the effect of increasing the Ge layer thickness is made difficult by the large standard deviation and the fact that the 15 nm Ge contacts showed microstructural discrepancies between the patterned TLM sample and the blanket sample used for the TEM study. However, all contacts containing Ge had low r_c -values, in the range 0.1 to 0.3 $\Omega \text{ mm}$, which are acceptable for OEIC applications.

3.2.2. I – V characteristics

The aim of the I – V (current–voltage) measurements was to test the applicability of the ohmic tunnelling theory [14] to the ohmic mechanism in the solid-state contacts. Hence, contacts A1 and S4, containing the largest amounts of Ge (that is, $x = 20 \text{ nm}$), were tested.

Both the as-deposited and the 270°C annealed contacts were ohmic at room temperature (Fig. 7a and d). They began to show rectifying characteristics as the temperature was decreased. The 270°C annealed contact continued to become more rectifying with decreasing temperature (Fig. 7e and f). In contrast, the rectifying behaviour of the as-deposited contact peaked at 150 K (Fig. 7b), becoming less rectifying at 100 K (Fig. 7c).

The tunnelling mechanism is essentially independent of temperature as tunnelling electrons need not overcome

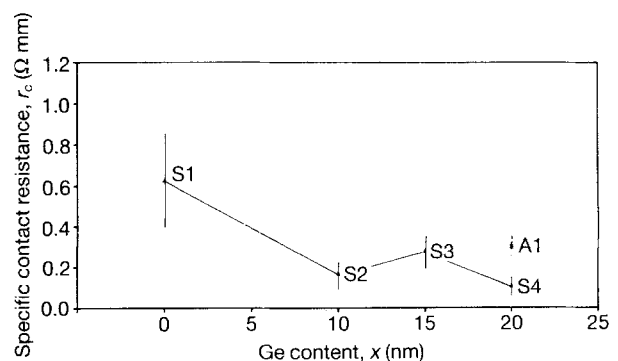


Figure 6 Variation of the specific contact resistance, r_c , of NiAuGe (5 nm/45 nm/ x nm)/ZBr₂(50 nm)/Au(20 nm) ohmic contacts to n-InGaAs with Ge content, x . A1: as-deposited S1, S2, S3, S4: annealed at 270°C. Microstructural discrepancies were observed between the TLM patterned and blanket TEM samples in contact S3.

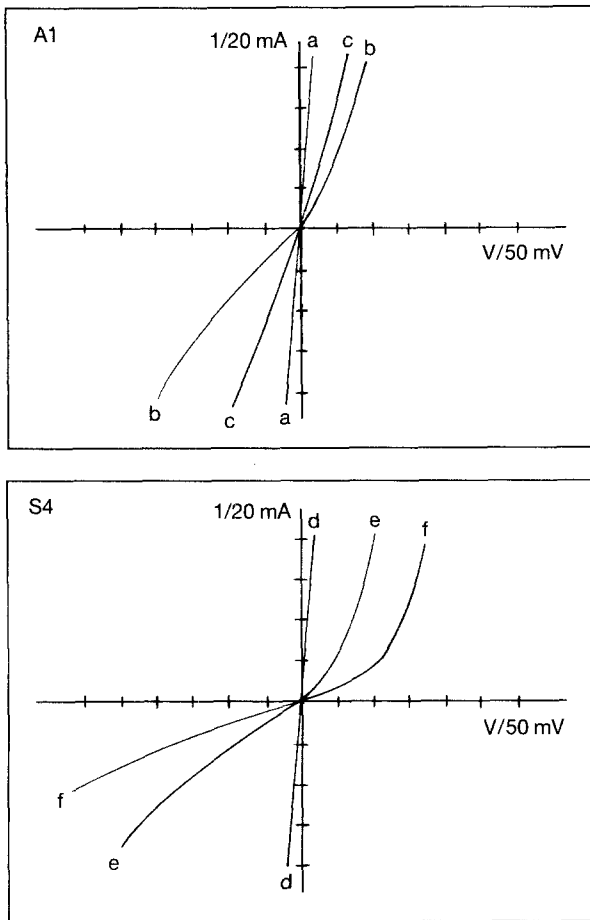


Figure 7 Low temperature I - V characteristics of contacts A1 (as-deposited) and S4 (annealed at 270°C) with 20 nm-thick layers. Contact A1: (a) room temperature, (b) 150 K, and (c) 100 K. Contact S4: (d) room temperature, (e) 150 K, and (f) 100 K.

the energy barrier at the metal-semiconductor interface. Fig. 7 shows that the I - V characteristics of both contacts were clearly temperature dependent. This indicates that the dominant ohmic mechanism was not tunnelling, and that current transport was at least partially thermionic.

The I - V characteristics of the as-deposited and annealed contacts are different from each other. This, however, is not surprising in view of their very different interfacial structures: in the as-deposited contact, a Ni layer was present at the interface; in the 270°C annealed contact, Au, NiGe and AuGeAs were all in contact with the InGaAs epilayer as well as there being Au penetration into the semiconductor.

In the case of the 270°C annealed contact, the microstructure is too complex for easy interpretation. However, in the case of the as-deposited contact, the ohmic properties may be explained in terms of pinning of the Fermi level, by Ni, close to the conduction band of the InGaAs [15].

4. Conclusions

1. The as-deposited NiAuGe (5 nm / 45 nm / 20 nm) / ZrB_2 (50 nm) / Au(20 nm) contact showed an unreacted layered microstructure. Its ohmic properties ($r_c = 0.3 \pm 0.05 \Omega\text{mm}$) are thought to result from Fermi-level pinning by the Ni layer.

2. The microstructures of annealed contacts are summarized in Table II. Ni-Ge-As was observed in the

contact with no Ge. This phase was replaced by Ni_2GeAs in the 10 nm Ge contact. On increasing the Ge content further, Ni_2GeAs was replaced by a Ni-Ge-As phase with a higher Ge content. In addition, increasing amounts of unreacted Ge and AuGeAs were observed, together with NiGe, at the metal-semiconductor interface.

3. The presence of NiGe at the metal-semiconductor interface was found to inhibit metal penetration into the semiconductor. All contacts had accepted penetration depths for OEIC applications (that is, < 100 nm) except for contact S2 (that is, 10 nm Ge), which had a penetration depth of 160 nm.

4. The highest specific contact resistance ($r_c = 0.63 \pm 0.23 \Omega\text{mm}$) was obtained for the contact without Ge. All the contacts containing Ge had low r_c -values acceptable for OEIC applications (that is, $r_c = 0.1$ - $0.3 \Omega\text{mm}$). Thus Ge is beneficial for ohmic properties.

5. Low-temperature I - V characteristics of the as-deposited and annealed contacts, A1 and S4, containing 20 nm thick Ge layers, indicated that tunnelling through a degenerately-doped InGaAs interfacial region is not the dominant ohmic mechanism.

Acknowledgement

The authors wish to thank Professor Malcolm McLean for the provision of experimental facilities in the Department of Materials, Imperial College.

References

1. O. WADA, T. SAKURAI and T. NAKAGAMI, *I.E.E.E. J. Quantum Electron.* **22** (1986) 905.
2. A. SUZUKI, K. KASAHARA and M. SHIKADA, *J. Lightwave Technol.* **5** (1987) 1479.
3. J. M. SENIOR, "Optical fibre communications; principle and practice" (Prentice-Hall, London, 1985).
4. D. A. ALLAN, J. HERNIMAN, M. J. GILBERT, P. J. O'SULLIVAN, M. P. GRIMSHAW and A. E. STATON-BEVAN, *J. Physique, C* **4** (1988) 427.
5. J. S. YU, A. E. STATON-BEVAN, J. HERNIMAN and D. A. ALLAN, Proceedings of the second International Conference on Electronic Materials, Newark, New Jersey, USA, September 1990, edited by T. Sugano, R. P. H. Chang, H. Kamimura, I. Hayashi and T. Kamiya (Materials Research Society, Pittsburgh, USA, 1991) p. 289.
6. X. ZHANG, PhD Thesis, University of London, 1987.
7. M. OGAWA, *Thin Solid Films*, **70** (1980) 181.
8. A. LAHAV, M. EIZENBERG and Y. YOMEN, Materials Research Society Symposium Proceedings, Vol. 37, edited by J. M. Gibson and L. R. Dawson (Materials Research Society, Pittsburgh, USA, 1985) p. 641.
9. T. SAND, V. G. KERMIDAS, A. J. YU, K.-M. YU, R. GRONSKY and J. WASHBURN, *J. Mater. Res.* **2** (1987) 262.
10. T. S. KUAN, P. E. BASTON, T. N. JACKSON, H. RUPPRECHT and E. L. WILKIE, *J. Appl. Phys.* **54** (1983) 6952.
11. M. P. GRIMSHAW and A. E. STATON-BEVAN, Institute of Physics Conference Series No. 93 Vol. 2, Proceedings of EUREM 88, York, UK, September 1988, edited by P. J. Goodhew and H. G. Dickinson (Institute of Physics Bristol, 1988) p. 113.
12. P. AUVRAY, A. GUIVARC'H, H. L'HARIDON, J. P. MERCIER and P. HENOC, *Thin Solid Films* **127** (1985) 39.
13. T. KIM and D. D. L. CHUNG, Materials Research Society Symposium Proceedings Vol. 54, edited by R. J. Nemanich *et al.* (Materials Research Society, Pittsburgh, USA, 1986) p. 439.
14. N. BRASLAU, J. B. GUNN and L. STAPLES, *Solid State Electron* **10** (1967) 381.
15. K. KAJIYAMA, Y. MIZUSHIMA and S. SAHATA, *Appl. Phys. Lett.* **23** (1973) 458.

Received 24 May

and accepted 26 August 1993